Crystal and magnetic structure investigation of $TbNi_{5-x}Cu_x$ ($x=0,0.5,1.0,1.5,2.0$): Experiment and theory

R. Lizárraga,[1] A. Bergman,[1] T. Björkman,[1] H.-P. Liu,[2] Y. Andersson,[2] T. Gustafsson,[2] A. G. Kuchin,[3] A. S. Ermolenko,[3] L. Nordström,[1] and O. Eriksson[1]

[1]*Department of Physics, Ångström Laboratory, Uppsala University, Box 530, S-751 21, Uppsala, Sweden*

[2]*Department of Materials Chemistry, Ångström Laboratory, Uppsala University, Box 538, S-751 21, Uppsala, Sweden*

[3]*Institute of Metal Physics, S.Kovalevskaya str. 18, 620219, Ekaterinburg, Russia*

(Received 13 April 2006; published 15 September 2006)

The effect of Cu substitution on the structural and magnetic properties of $TbNi_{5-x}Cu_x$ ($x=0,0.5,1.0,1.5,2.0$) have been investigated by x-ray diffraction, magnetization measurements and neutron powder and single crystal diffraction. The electronic and the magnetic structures of $TbNi_5$ were studied using first principles theory. All samples were found to have the $CaCu_5$-type structure, space group $P6/mmm$. The lattice parameters increase monotonically with increasing Cu concentration. The Curie temperature T_c has a maximum value of 29 K at $x=1.0$. The magnetic structure of $TbNi_5$ at 10 K is incommensurate with a helimagnetic component [wave vector $\mathbf{q}\sim 2\pi/c(0,0,0.02)$] perpendicular to a ferromagnetic one. In contrast, the substituted $TbNi_{5-x}Cu_x$ alloy is ferromagnetic. All magnetic moments are observed to be located on the Tb atoms. The magnetocrystalline anisotropy in the *ab* plane is observed to be strongly increased by the Cu substitution, whereas the magnetization decreases with the Cu concentration. The observed magnetic structure of $TbNi_5$ is consistent with first principles calculations regarding both the magnetic moments and the helimagnetic structure. The microscopical origin of the helimagnet is analyzed and correlated to the Fermi surface topology.

DOI: 10.1103/PhysRevB.74.094419 PACS number(s): 75.50.Cc, 71.20.Be, 71.55.Ak

I. INTRODUCTION

The high symmetry of the crystal structure that the RNi_5 series (R=rare earth) possess and the richness of their magnetic structure have stimulated several detailed studies of these compounds.[1] Single crystals of $TbNi_5$ have previously been investigated by means of magnetization,[2] resistivity,[3] NMR,[4] XMCD,[5] μSR (Ref. 6) and inelastic neutron scattering experiments.[7] However, very few theoretical studies of these compounds have been reported.[8]

$TbNi_5$ crystallizes in the hexagonal $CaCu_5$-type structure (space group $P6/mmm$) (Ref. 9) with one formula unit per unit cell. There are one Tb site ($1a$) and two nonequivalent Ni sites, Ni1($2c$) and Ni2($3g$). $TbNi_5$ has a strong magnetocrystalline anisotropy with an easy *ab* plane and a hard *c* axis.[10,11] The anisotropy in the *ab* plane is small. From magnetic susceptibility and magnetization measurements on a polycrystalline sample of $TbNi_5$, Barthem *et al.*[12] proposed that there exists a helimagnetic phase between $T_h=17$ K and $T_N=23$ K when $H<400$ Oe. For $T<T_h$ the compound exhibits ferromagnetic behavior, at any applied field. Moreover, Barthem *et al.* also reported that in the Cu substituted $TbNi_{5-x}Cu_x$ compounds there is a helimagnetic ordering in a narrow temperature range of 6 K at fields smaller than a critical field. At even lower temperatures, the compounds are reported to be ferromagnetically ordered.[13] Recently, neutron diffraction experiments were performed on $TbNi_5$ (Refs. 14 and 15) in the temperature range 2.2–30 K. The magnetic structure was described in terms of a fanlike structure with two wave vectors [$k_1=0$ and $k_2=2\pi/c(0,0,0.019)$]. The ferromagnetic component of the magnetic moment on Tb was found to be $8.4\mu_B$ and a helical part of $5.1\mu_B$ at 2.2 K which gives a total moment of $9.8\mu_B$. Kuchin *et al.*[16] studied the magnetic properties and heat capacity of $TbNi_{5-x}M_x$ (M=Cu, Al) for $x\leqslant 2.5$ and $x\leqslant 1.5$, respectively. However, the magnetic structures of the substituted intermetallic $TbNi_{5-x}Cu_x$ alloys have not been finally determined and this motivates an extended theoretical or experimental investigation of this interesting material. In the present study, neutron diffraction experiments and magnetization measurements have been performed in parallel to first principles theory of the electronic structure and magnetic properties. The site occupancies and the magnetic ordering have been determined experimentally. Our theoretical analysis has identified nesting behavior as the main reason for the magnetic ordering.

II. EXPERIMENTS

Syntheses. $TbNi_{5-x}Cu_x$ ($x=0.0,0.5,1.0,1.5,2.0$) samples were synthesized by induction melting of appropriate amounts of the elements in an argon atmosphere. The as-cast ingots were sealed in evacuated quartz tubes and annealed at 1373 K for 2 days, then quenched into water. Single crystals of $TbNi_{5-x}Cu_x$ ($x=0.5,1.0$) were prepared by the Czochralski method in a crucible in an induction furnace. The crystal shapes were a 2.7 mm diameter sphere and a $3\times 3\times 3$ mm^3 cube, respectively.

Phase analysis. X-ray diffraction patterns showed that the powder samples were single phase with the hexagonal $CaCu_5$-type structure. The unit cell parameters were determined by least-square refinements from scanned Guinier-Hägg photographs (Cu $K\alpha_1$ radiation) using high purity silicon as internal standard.

Magnetization measurements. The spontaneous magnetization at $T=4.2$ K was deduced from magnetization curves

measured along the easy direction of the single crystals up to a field of 7 T by means of a vibrating-sample magnetometer. The Curie temperatures were determined from the temperature dependence ($4.2<T<50$ K) of the initial ac susceptibility.

Neutron diffraction. Neutron diffraction measurements were performed at the Swedish *R*2 reactor in Studsvik. For the powder experiment, high flux monochromated neutrons of wavelength 1.47 Å were obtained from the (220) planes of two parallel Cu single crystals. Powder diffraction intensities were collected at 40 K, 30 K, 25 K, 20 K, 15 K, and 10 K for $TbNi_5$; at 40 K, 10 K for $TbNi_{4.5}Cu_{0.5}$ and $TbNi_4Cu$, and at 40 K, 25 K, 10 K for $TbNi_{3.5}Cu_{1.5}$ and $TbNi_3Cu_2$ by a 35 multidetector system scanning over the 2Θ range 4.00°–139.93° in steps of 0.08°. Neutron single crystal data were collected on a four-circle Huber single-crystal diffractometer at 295 K using an incident wavelength of 1.207 Å. Three standard reflections were used to check the stability of the instrument and the quality of the collected intensities. The available cryostat used at the single crystal diffractometer could only reach a minimum temperature of 25 K; the low temperature measurements were therefore performed on powder samples.

Structure refinements. All the structure refinements were made using the program FULLPROF.[17] The collected intensities from the single crystals were corrected for Lorentz and absorption effects. Scale factor, occupancy and extinction correction factor were refined based on 99 reflections using the full-matrix least-squares method. The calculated intensities are significantly higher than those of the observed values for the strong reflections, indicating the existence of extinction effect. The powder data were analyzed by means of the Rietveld profile procedure[18] with the atomic scattering lengths, $b_{Tb}=7.38$ fm, $b_{Ni}=10.3$ fm, $b_{Cu}=7.72$ fm. In the 10 K data refinements, the magnetic moment of Tb was refined together with a scale factor, two unit cell parameters, and five profile parameters, while the site occupancies were fixed at the values obtained at 40 K.

III. THEORETICAL METHOD

In the present theoretical study we treated the 4*f* states in Tb as part of the core which reflects their localized nature, while they are still able to produce an exchange field that acts on the valence states. In order to simulate the experimental situation, the 4*f* states have been spin-polarized among the core states. The spin occupation numbers are determined by applying Russel-Saunders coupling[19] to the 4*f* shell. This scheme allows for accurate first principles description of the indirect exchange coupling of the RE spin moments.[20]

The spin spiral (SS) symmetry has been adopted in order to handle planar and canted helical spin structures, where the parallel spins within a plane are rotating around the hexagonal axis with an angle $\phi=qc$ between each hexagonal Tb plane. The magnetization density of a SS is not translational invariant along the propagation direction. Therefore a supercell is generally used when performing calculations. However a generalized boundary condition[21] can be used in order to restore the chemical unit cell

$$\mathbf{m}(\mathbf{r}+\mathbf{R})=\mathcal{D}(\mathbf{q}\cdot\mathbf{R})\mathbf{m}(\mathbf{r}), \tag{1}$$

where $\mathbf{R}$ is a Bravais lattice vector, $\mathbf{q}=(0,0,q)$ is the wave vector of the SS and $\mathcal{D}(\mathbf{q}\cdot\mathbf{R})$ is a matrix that accomplishes a rotation of the in-plane component of $\mathbf{m}$ by the angle $\mathbf{q}\cdot\mathbf{R}$ around the hexagonal axis. The generalized Bloch spinor states[22,21] can then be written as

$$\psi(\mathbf{k},\mathbf{r})=e^{i\mathbf{k}\cdot\mathbf{r}}\begin{pmatrix} e^{-i\mathbf{q}/2\cdot\mathbf{r}}\alpha(\mathbf{k},\mathbf{r}) \\ e^{+i\mathbf{q}/2\cdot\mathbf{r}}\beta(\mathbf{k},\mathbf{r}) \end{pmatrix},$$

where $\mathbf{k}$ is a wave vector in the Brillouin zone (BZ) and α and β are the periodic functions for the spin-up and spin-down components, respectively. The secular matrix constructed from theses states is no longer block diagonal which means that the two spin components can hybridize. Self-consistency is achieved by constructing new charge and magnetization densities from the occupied Bloch spinors.[23] Thus, this scheme is specially suited to study incommensurate structures.

In our investigation we have used two methods, the full-potential augmented plane wave (FP-APW+lo) (Refs. 24 and 25) and the LMTO-ASA.[26] The noncollinear scheme described above is implemented in both methods. The FP-APW+lo method allowed us to calculate accurate total energies and resolve the magnetic and electronic structure. Fermi surfaces were calculated by using the LMTO-ASA. The faster LMTO-ASA affords a larger set of *k* points without the calculations becoming intractable, and thus improving the resolution for the Fermi surface. The local spin

TABLE I. The unit cell parameters at 295 K, T_c and the magnetization M_s at 4.2 K of $TbNi_{5-x}Cu_x$. Estimated standard deviations are given in parentheses.

Compounds	a (Å)	c (Å)	V (Å^3)	T_c (K)	M_s (μ_B/f.u.)
$TbNi_5$	4.8988(2)	3.9600(2)	82.30(1)	25	7.7
$TbNi_{4.5}Cu_{0.5}$	4.9049(2)	3.9752(2)	82.82(1)	27	6.8
$TbNi_4Cu$	4.9126(2)	3.9901(2)	83.39(1)	29	6.2
$TbNi_{3.5}Cu_{1.5}$	4.9274(2)	3.9988(3)	84.08(1)	28	6.3
$TbNi_3Cu_2$	4.9351(2)	4.0113(2)	84.61(1)	25	6.2

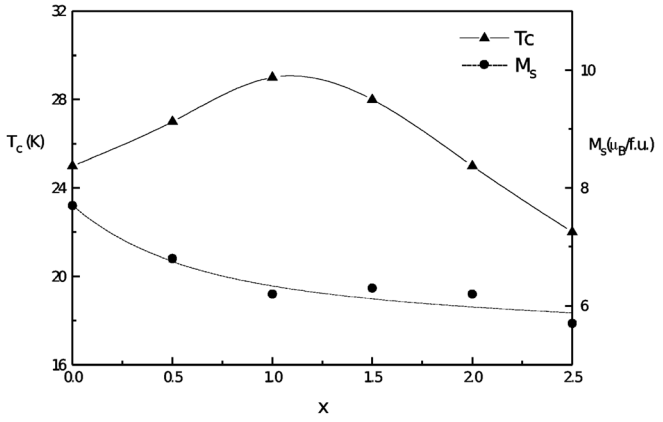

FIG. 1. The magnetic moments at 4.2 K and the Curie temperature of $TbNi_{5-x}Cu_x$.

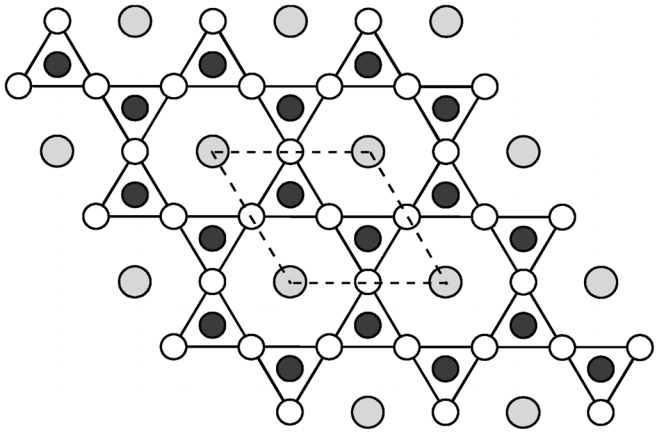

Atom	Site	x	y	z
Tb	(1a)	0	0	0
Ni1	(2c)	1/3	2/3	0
Ni2	(3g)	1/2	0	1/2

FIG. 2. The crystal structure of $TbNi_5$ projected on the *ab* plane.

density approximation (LSDA) as parametrized by von Barth and Hedin[27] was used. The calculations have been performed for the hexagonal structure of $TbNi_5$, at the experimental lattice constants, *a* and *c*. Brillouin zone (BZ) integrations obtained by FP-APW+lo were performed using a mesh of 220 *k* points in the irreducible BZ, together with a temperature broadening of k_BT=5 mRy. For the LMTO-ASA calculations a mesh of 2244 *k* points in the IBZ and a broadening of 0.5 mRy were used.

IV. EXPERIMENTAL RESULTS

The substitution of Ni by Cu results in an increase of the unit cell volume. The lattice constants, the saturation magnetization M_s at 4.2 K and the Curie temperature T_c are listed in Table I. In Fig. 1, the Curie temperature curve presents a maximum at x=1.0 and the saturation magnetization decreases with the Cu content. There is no obvious correlation between T_c and the magnetic moments. The projection of the $TbNi_5$ crystal structure on the (001) plane is shown in Fig. 2. The Tb atoms are surrounded by six nearest Ni_1 atoms in the *ab* plane and 12 next nearest Ni_2 atoms at $z=\pm 1/2c$. Interatomic distances are listed in Table II. The occupancies of Cu on the two different Ni positions were determined from neutron data at 40 K (see Table III). For $x<1.0$ the Cu atoms have a slight preference to enter the Ni_1 position, while for $x\geqslant 1.0$ a preference of occupying the Ni_2 position occurs. It is worth noting that the concentration dependence of site occupancies has the same trend as T_c with a turning point at x=1.0. As previously reported,[28] T_c is associated with the crystalline electric field (CEF) effect on the terbium atoms, which originates from the electric charge difference of the statistical mixture of Ni and Cu on the same site. A larger CEF on the Tb atoms is created due to shorter distances between Tb and Ni_1, and accompanying this reduced Tb-Ni distance is an increased T_c. However, increased Cu substitu-

TABLE II. Interatomic distances in $TbNi_{5-x}Cu_x$ at 295 K. Distances listed are less than 3.2 Å for Ni-Ni and Ni-Tb and less than 5.0 Å for Tb-Tb.

	$TbNi_5$ *d* (Å)	$TbNi_{4.5}Cu_{0.5}$ *d* (Å)	$TbNi_4Cu$ *d* (Å)	$TbNi_{3.5}Cu_{1.5}$ *d* (Å)	$TbNi_3Cu_2$ *d* (Å)
Ni1–6 Ni2	2.433	2.440	2.448	2.454	2.460
Ni1–3 Ni1	2.828	2.832	2.836	2.845	2.849
Ni1–3 Tb	2.828	2.832	2.836	2.845	2.849
Ni2–4 Ni1	2.433	2.440	2.448	2.454	2.460
Ni2–4 Ni2	2.449	2.452	2.456	2.464	2.468
Ni2–4 Tb	3.150	3.157	3.164	3.173	3.180
Tb–6 Ni1	2.828	2.832	2.836	2.845	2.849
Tb–12 Ni2	3.150	3.157	3.164	3.173	3.180
Tb–2 Tb	3.960	3.975	3.990	3.999	4.011
Tb–6 Tb	4.8998	4.905	4.913	4.927	4.935

TABLE III. The refined Ni/Cu occupancies of $TbNi_{5-x}Cu_x$ with agreement factors.

	$TbNi_{4.5}Cu_{0.5}$		$TbNi_4Cu$			
Compounds	Powder	SC[a]	Powder	SC[a]	$TbNi_{3.5}Cu_{1.5}$ Powder	$TbNi_3Cu_2$ Powder
Occ. Cu1 $(2c)$[b]	0.22(2)	0.25(4)	0.40(2)	0.37(5)	0.53(2)	0.75(2)
Fraction occ. (%)[c]	11	12	20	19	27	38
Occ. Cu2 $(3g)$[b]	0.28(2)	0.25(4)	0.60(2)	0.61(5)	0.97(2)	1.25(2)
Fraction occ. (%)[c]	9	8	20	20	32	42
$R_f(\%)$	2.48	4.37	2.91	4.88	3.07	3.11
$R_p(\%)$	3.70	6.79[d]	3.90	6.95[d]	4.17	3.99
$R_{wp}(\%)$	4.77	9.74[e]	4.86	8.56[e]	5.40	4.98
$R_{\exp}(\%)$	2.59		2.79		2.76	2.99
$R_{\text{Bragg}}(\%)$	3.47		4.72		5.07	5.06

[a]Single crystals measured at 295 K.
[b]The number of Cu atoms occupied on Ni/Cu position.
[c]The fraction of full occupancy (%).
[d]$R(F^2)(\%)$.
[e]$wR(F^2)(\%)$.

tions lead to longer Tb-Ni_2 distances, which results in smaller CEF on the Tb atoms and consequently T_c decreases. The same results were obtained from powder and single crystal neutron diffraction experiments.

The neutron powder diffractogram at 10 K of $TbNi_5$ in Fig. 3 shows satellites around the $(h\ k\ l)$ reflections with $l \neq 0$, which indicates the formation of an incommensurate helimagnetic ordering. The $\pm(000)$ reflection is almost completely overlapped with the primary beam (see the inset in Fig. 3). The diffraction patterns were fitted with an incommensurate structure which was resolved into a helimagnetic component perpendicular to a ferromagnetic one. The satellite reflections were indexed by a propagation vector $\mathbf{q}=(0,0,0.0195(3))$ in excellent agreement with previous experiments.[14] The preliminary results indicate that the ferromagnetic component of the magnetic moment was $7.16(1)\mu_B$/Tb atom in the *ab* plane and the helical part $4.5(1)\mu_B$/Tb atom. These two components of the magnetic moment are smaller than the moments obtained in Ref. 14. The total magnetic moment $8.4\mu_B$/Tb atom was obtained with the half-cone-angle (32°) to the [1 0 0] helical axis, and the spins are rotated 7.0(1)° between successive magnetic sheets projected on the *ab* plane. The Ni atoms do not carry any significant moment. The ferromagnetic contribution of the Tb moments roughly agrees with the magnetization measurements. The magnetization measurements at 4.2 K under the applied magnetic field 7 T give a somewhat higher value ($7.7\mu_B$/Tb atom) than that obtained from the neutron powder diffraction measurements at 10 K without any external field. If we estimate the total magnetic moment based on this number for the moment in the *ab* plane together with the helical component of $4.5\mu_B$ that was obtained from the neutron diffractogram, a total moment of $\sim 8.9\mu_B$/Tb atom is found. This moment is what one would expect in Russel-Saunders coupling for a Tb atom in a $4f^8$ configuration but somewhat smaller than in Ref. 14. An illustration of the magnetic spin orientation of $TbNi_5$ is shown in Fig. 4. All the Cu substituted $TbNi_{1-x}Cu_x$ $(x=0.5,1.0,1.5,2.0)$ samples are ferromagnetic, according to neutron powder diffraction patterns at 10 K. The magnetic scattering intensities were imposed on the nuclear reflections. We did not find any helimagnetic ordering at 25 K in $TbNi_{3.5}Cu_{1.5}$ nor in $TbNi_3Cu_2$, which is in contradiction to the earlier proposed helimagnetic ordering existing in the temperature range between T_h and T_N.[13] There was no significant magnetic moments observed on the Ni/Cu atoms. The magnetic moments were found to be located on the Tb atoms with the magnetic spin in the *ab* plane. The calculated and observed neutron powder diffraction profiles at 10 K for $TbNi_{5-x}Cu_x$ $(x=0.5,1.5)$ are shown in Fig. 5. The contributions of the magnetization arise from the Tb $4f$ electrons that couple ferromagnetically. Ni is nearly nonmagnetic due to the almost complete filling of the $3d$ shell by the $5d$ electrons of Tb. At higher Cu concentrations, the average atomic distances increase, therefore the magnetic interaction between the Tb atoms becomes weaker. As seen in Table IV, the magnetic moments on the Tb atoms decrease with increasing Cu content, which is consistent with the result from magnetization measurements in Fig. 1.

V. THEORETICAL RESULTS

A. Electronic structure

The calculated density of state (DOS) of the valence band is shown in Fig. 6. The occupied part of the DOS is dominated by Ni *d* states whereas the Tb *d* states form a background to the DOS without much structure. The main features of the Tb *d* states are located above the Fermi level. It can be seen in Fig. 6 that there is a small exchange splitting of the valence band states, which is consistent with the small induced moment caused by the $4f$-$5d$ exchange interaction, that via hybridization is mediated also to the Ni states. The energy band dispersion is depicted in Fig. 7 for a ferromagnetic configuration. It may be seen that most energy bands

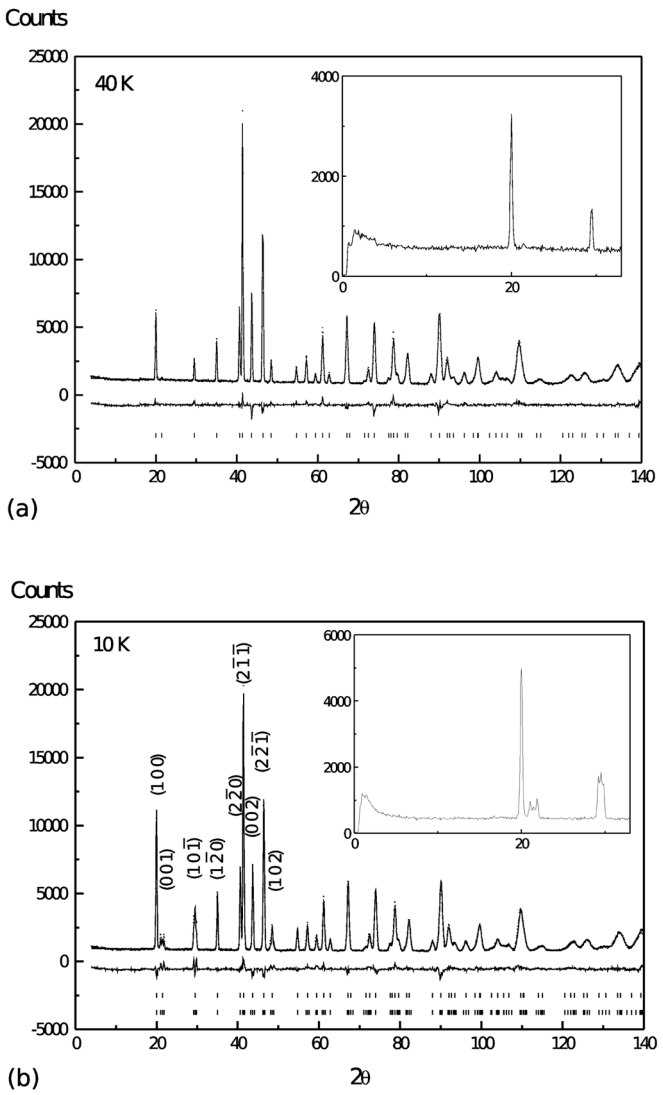

FIG. 3. Observed and calculated neutron diffraction patterns $TbNi_5$ at 40 K (a) and 10 K (b). The insets show the low 2θ range. The difference line is shown at the bottom of each figure.

come in pairs that are separated with a small energy, which is the result of a small exchange splitting induced by the moment of the localized $4f$ electrons. This actually has relevance for the magnetic structure and we will return to this discussion below.

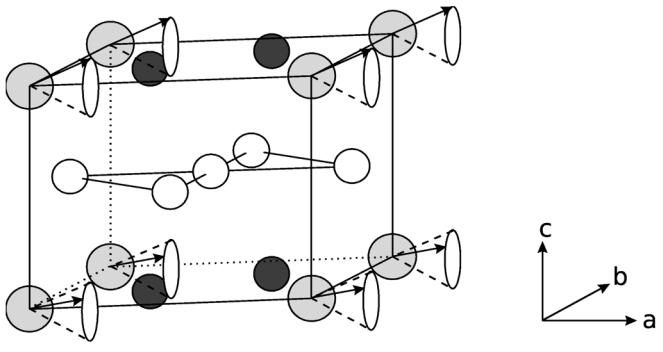

FIG. 4. The helimagnetic structure of $TbNi_5$.

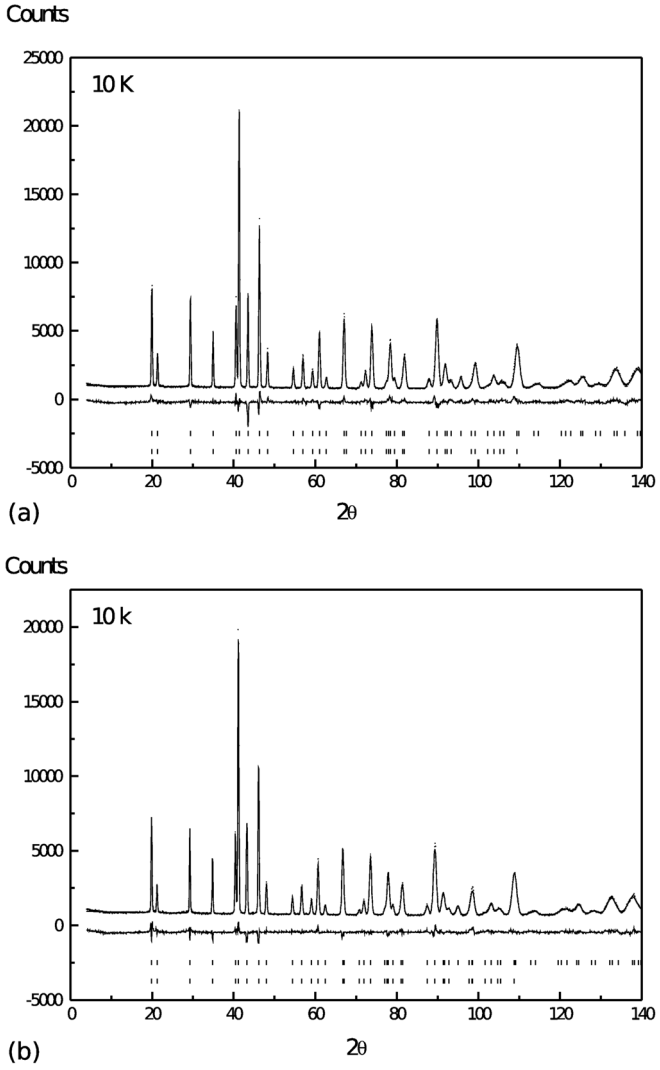

FIG. 5. Observed and calculated neutron diffraction patterns at 10 K for $TbNi_{4.5}Cu_{0.5}$ (a) and $TbNi_{3.5}Cu_{1.5}$ (b). The difference line is shown at the bottom of each figure.

B. Magnetism

Different spin spiral wave vectors **q** in the (0,0,1) direction of the hexagonal Brillouin zone have been investigated. The calculated total energy as a function of the z component of the helical ordering **q** vector is displayed in Fig. 8. The ordering vectors $\mathbf{q}=(0,0,0)$ and $\mathbf{q}=(0,0,1/2)2\pi/c$ correspond to the ferromagnetic and the antiferromagnetic order, respectively. The curve in Fig. 8 presents a minimum at $\mathbf{q}=(0,0,0.06)2\pi/c$, which means that a noncommensurate helical magnetic structure is more stable than the ferromagnetic and antiferromagntic configuration. Unfortunately, the agreement with the experimental value, $q=0.02$, is not perfect. The small energy difference ~ 0.11 mRy/f.u. between the ferromagnetic state and the calculated spin spiral at $q=0.06$ shows that the formation of the spin spiral in this compound is the result of an extremely delicate equilibrium of competing phenomena.

The total moment of the $4f$ shell, according to Hund's rules, was determined by $\mathbf{J}=\mathbf{L}+\mathbf{S}$,[19] and amounts to a mo-

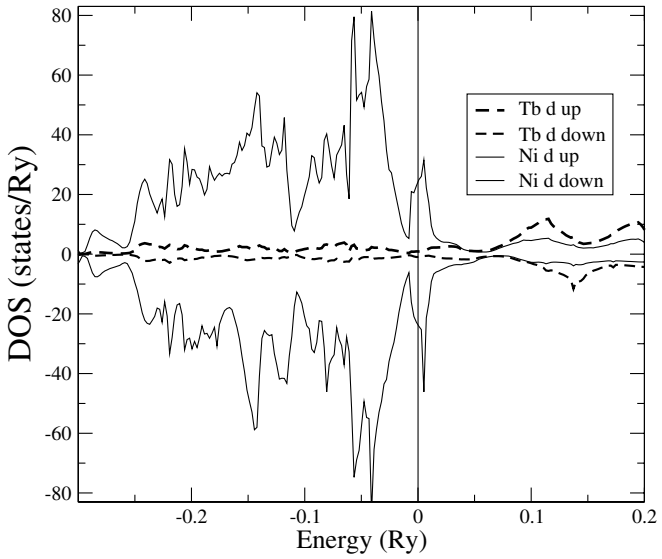

FIG. 6. Density of states of $TbNi_5$. The Fermi energy is at zero energy and is marked by a vertical line.

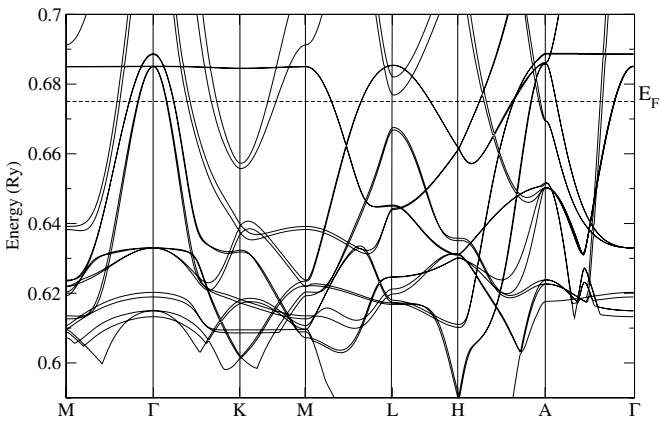

FIG. 7. Band structure of $TbNi_5$. The Fermi energy is marked by a dashed horizontal line.

ment of $9\mu_B$. The calculated valence band moment can be decomposed onto atomic sites and an interstitial contribution. The so calculated moments depend, to some extent, on the choice of the muffin-tin radii. In the present calculation we obtain a very small moment from the valence band states, that can be decomposed to a positive contribution from the interstitial region ($\sim 0.4\mu_B$/f.u.) and a negative contribution from the Ni and Tb muffin tins ($\sim 0.4\mu_B$/f.u.). Hence the total magnetic moment is close to 9 in our theory. This should be compared to the experimentally deduced values of $8.4\mu_B$/f.u. and $8.9\mu_B$/f.u., where obviously the latter value is in better agreement with theory.

C. Fermi surface

To explain the origin of the observed magnetic spin spiral structure we have calculated the Fermi surface of $TbNi_5$, in order to analyze possible nesting features of the valence band electronic structure. In Fig. 9 we show the calculated nonmagnetic Fermi surface. In this figure one may observe two almost parallel Fermi sheets which are connected by a **q** vector. Already in earlier studies of magnetic structures of rare earths[23,29,30] serious evidences of the existence of a relation between the **q** vector of the magnetic structure and the Fermi surface nesting was observed. Normally, this is expected since the generalized susceptibility becomes large for q values corresponding to the nesting vector. In the present case this analysis cannot explain the observed magnetic structure, since the nesting features shown in Fig. 9 are expected to result in a spin-spiral with a q value much larger than the observed and calculated values.

As an alternative explanation, strong nesting between spin-up and spin-down Fermi surfaces of a ferromagnetic configuration has been discussed in the past as an indicator of instabilities of the ferromagnetic state against the formation of a spin spiral[31,32] and we will proceed with an analysis based on these arguments. First we observe that the modification of the energy band structure is rather small when comparing the nonmagnetic configuration and the ferromagnetic configuration. As noted in Fig. 7 the band structure is essentially intact with a small exchange splitting between the

TABLE IV. The final magnetic structure data at 10 K for $TbNi_{5-x}Cu_x$. Estimated standard deviations are given in parentheses.

Compounds	$TbNi_5$	$TbNi_{4.5}Cu_{0.5}$	$TbNi_4Cu$	$TbNi_{3.5}Cu_{1.5}$	$TbNi_3Cu_2$
M_x (μ_B)	7.16(1)	6.88(6)	6.18(6)	5.88(6)	5.47(6)
M_z (μ_B)	4.51 (1)	0	0	0	0
k	(0,0, 0.0195(3))	(0,0,0)	(0,0,0)	(0,0,0)	(0,0,0)
a (Å)	4.8869(3)	4.8921(2)	4.9003(2)	4.9130(2)	4.9231(2)
c (Å)	3.9501(2)	3.9657(1)	3.9809(1)	3.9899(1)	4.0019(1)
R_p(%)	4.63	4.77	4.41	4.31	4.73
R_{wp}(%)	6.11	6.32	5.61	5.51	6.22
R_{exp}(%)	2.64	2.69	2.89	2.78	2.98
R_{Bragg}(%)	5.63	5.72	5.45	4.31	6.20
R_{magn}(%)	12.2	5.68	5.63	7.81	6.06

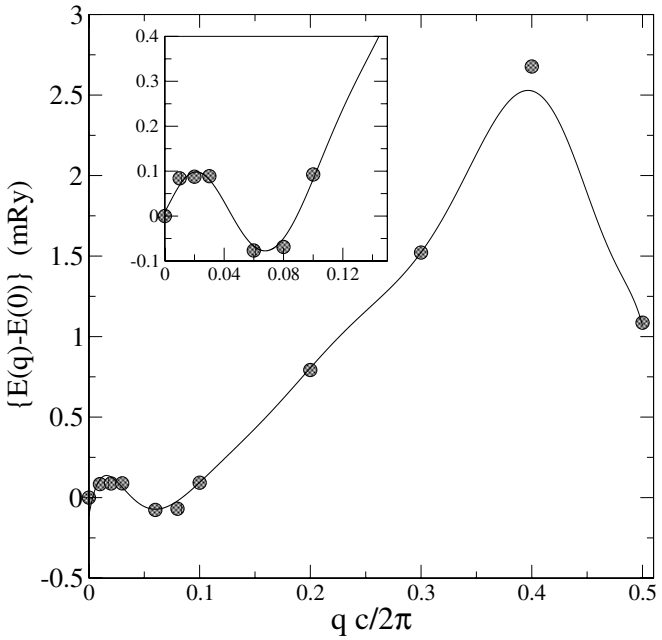

FIG. 8. The calculated total energy as a function of the spin spiral wave vector $\mathbf{q}=(0,0,q)$ in units of $2\pi/c$ is depicted (grey dots, the line is just a guide to the eye). In the inset we show an enlarged figure around the low-q region.

spin-up and spin-down bands, which induces a small shift between the spin-up and spin-down sheets of the Fermi surface. The result is a spin-up and a spin-down Fermi surface (not shown) that are very similar to the one shown in Fig. 9, but with a small shift in q space between them. The shift between the spin-up and spin-down surfaces is expected to result in very strong nesting features in the z axis of reciprocal space, since Fig. 9 shows large planar sections of the Fermi surface with a normal that points in the z direction of reciprocal space. This nesting might explain the magnetic structure.

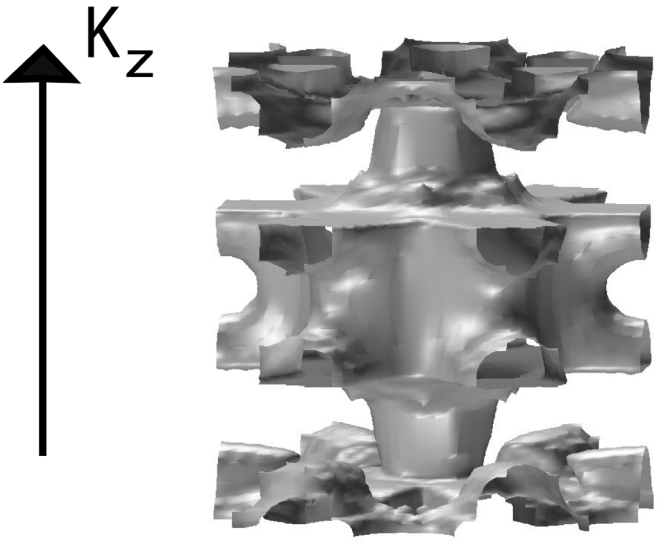

FIG. 9. Calculated Fermi surface of the paramagnetic phase of $TbNi_5$.

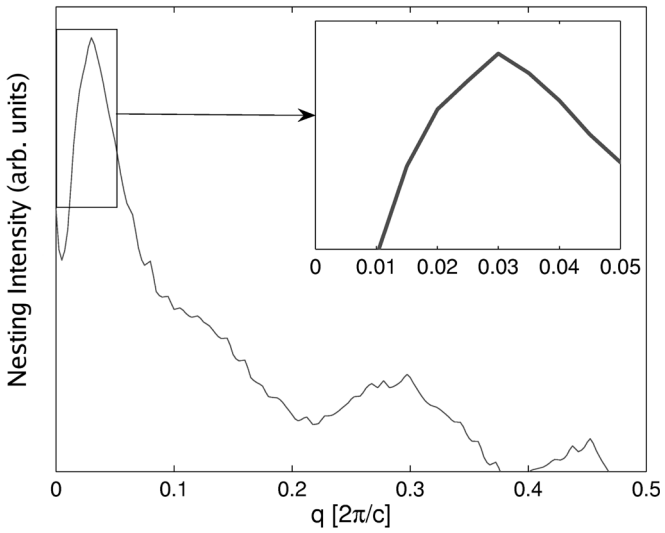

FIG. 10. Calculated nesting intensity of $TbNi_5$ (for details see, text). In the inset a blown up region around $q\sim 0$ is shown.

In order to explore this possibility we extrapolated the k-point mesh to a uniform $100\times 100\times 200$ mesh, and in this way both the spin-up and spin-down sheets of the Fermi surface were extracted. Each sheet was found to consist of $\approx 50\,000$ points on the mesh. For each point on the spin-up surface, all vectors along the z axis, $\mathbf{q}=(0,0,z)$ connecting to the spin-down surface were identified. Thus, we defined a nesting intensity as a function of the vector length $|\mathbf{q}|=z$ that can be obtained by summing over all points on the spin-up surface. The result is shown in Fig. 10 where the number of coinciding points are shown as a function of the size of the displacement, $|\mathbf{q}|=z$. It can be seen in this figure that there is a large peak at $\mathbf{q}=2\pi/c(0,0,0.03)$, which shows that there are strong nesting features corresponding to a $\mathbf{q}$ vector that is quite close to the $\mathbf{q}$ vector of the magnetic structure.

VI. CONCLUSION

We have synthesized alloys of $TbNi_{5-x}Cu_x$ $(x=0,0.5,1.0,1.5,2.0)$ that form in the $CaCu_5$-type structure. The magnetic structure has been characterized by neutron diffraction experiments. For $TbNi_5$ the magnetic structure is incommensurate with a very small q value along the [001] direction; it presents a helimagnetic component perpendicular to a ferromagnetic one. This structure disappears as a function of alloying with Cu and a ferromagnetic phase occurs instead. The measured total moment of $TbNi_5$ is $8.4-8.9\mu_B$/Tb atom, which compares well with the calculated value of $\sim 9\mu_B$/Tb atom.

The magnetic helix is consistent with a minimum at $\mathbf{q}=2\pi/c(0,0,0.06)$ in the calculated total energy. Considering the very small energies involved for determining the stability of different magnetic structures around $q=0$, one must conclude that theory reproduces experimental observations with a rather decent accuracy. The observed magnetic structure can be explained from the calculated electronic structure of

$TbNi_5$, where we observe a pronounced nesting feature between spin-up and spin-down sheets of the Fermi surface for $q=0.03$ along the [001] direction.

Hence one must conclude that theory and experiment agree rather well concerning the magnetic properties of $TbNi_5$. Nevertheless, certain aspects of the observed magnetic structure have not been possible to address theoretically. For instance the fact that the main component of the magnetization lies in the *ab* plane due to the magnetic anisotropy has not been possible to verify theoretically, since this requires the inclusion of spin-orbit splitting in combination with a wave function that has the symmetry of a helix structure, something which at present is not possible to do.

ACKNOWLEDGMENTS

The authors would like to thank Håkan Rundlöf for skillful assistance with the neutron diffraction measurement. Support of the Swedish Research Council (VR) and the Swedish Foundation for Strategic Research (SSF) is gratefully acknowledged. The authors also acknowledge support from the Swedish National Super Computer facility (NSC).

[1] J. Jensen and A. R. Mackintosh, *Rare Earth Magnetism* (Clarendon, Oxford, 1991).
[2] J. J. M. Franse and R. J. Radvansky, in *Ferromagnetic Materials*, edited by K. H. J. Buschow (North-Holland, Amsterdam, 1993), Vol. 7.
[3] J. A. Blanco, D. Gignoux, D. Schmitt, A. Tari, and F. Y. Zhang, J. Phys.: Condens. Matter **6**, 4335 (1994).
[4] C. Carboni, D. Gignoux, and A. Tari, Phys. Rev. B **52**, 9486 (1995).
[5] Carboni, D. Gignoux, Y. Li, J. W. Ross, and A. Tari, J. Phys.: Condens. Matter **8**, 1763 (1996).
[6] R. M. Galera and A. Rogalev, J. Appl. Phys. **85**, 4889 (1999).
[7] P. Dalmas de Reotier, A. Yaouanc, P. C. M. Gubbens, D. Gignoux, B. Gorges, D. Schmitt, O. Hartmann, R. Wäppling, and A. Weidinger, J. Magn. Magn. Mater. **104-107**, 1267 (1992).
[8] G. E. Grechnev, V. A. Desnenko, A. S. Panfilov, I. V. Svechkarev, P. E. Brommer, J. J. M. Franse, and F. E. Kayzel, Physica B **237-238**, 532 (1997).
[9] J. H. Warnick and S. Geller, Acta Crystallogr. **12**, 662 (1959).
[10] D. Gignoux, A. Nait-saada, and R. Perrier de la Bathie, J. Phys. (Paris), Colloq. **40**, C5-188 (1979).
[11] P. A. Algarabel, L. Morellon, M. R. Ibarra, D. Schmitt, D. Gignoux, and A. Tari, J. Appl. Phys. **73**, 6054 (1993).
[12] V. M. T. S. Barthem and E. A. Moreira da Gama, J. Phys.: Condens. Matter **9**, 7609 (1997).
[13] V. M. T. S. Barthem, E. A. Moreira da Gama, and A. Y. Takeuchi, J. Magn. Magn. Mater. **177-181**, 1065 (1998).
[14] S. Lee, A. N. Pirogov, J.-G. Park, I. P. Swainson, Yu. A. Dorofeev, A. E. Teplykh, A. S. Ermolenko, E. G. Gerasimov, and A. A. Podlesnyak, Europhys. Lett. **62**, 350 (2003).
[15] S. Lee, A. A. Podlesnyak, K. Prokes, V. E. Sikolenko, A. S. Ermolenko, E. G. Gerasimov, Yu. A. Dorofeev, A. P. Vokhmyanin, J.-G. Park, and A. N. Pirogov, JETP Lett. **82**, 34 (2005).
[16] A. G. Kuchin, A. S. Ermolenko, V. I. Khrabrov, N. I. Kourov, G. M. Makarova, Ye. V. Belozerov, T. P. Lapina, and Yu. A. Kulikov, J. Magn. Magn. Mater. **238**, 29 (2002).
[17] J. Rodrigues-Carvajal, FULLPROF version 3.2, January 1997.
[18] H. M. Rietveld, J. Appl. Crystallogr. **2**, 65 (1969).
[19] D. Craik, *Magnetism: Principles and Applications* (Wiley, New York, 1998).
[20] M. S. S. Brooks, L. Nordström, and B. Johansson, J. Phys.: Condens. Matter **3**, 2357 (1991).
[21] L. Sandratskii, Adv. Phys. **47**, 91 (1998).
[22] C. Herring, *Magnetism* (Academic, New York, 1966).
[23] L. Nordström and A. Mavromaras, Europhys. Lett. **49**, 775 (2000).
[24] E. Sjöstedt, L. Nordström, and D. Singh, Solid State Commun. **114**, 15 (2000).
[25] E. Sjöstedt and L. Nordström, Phys. Rev. B **66**, 014447 (2002).
[26] The computer code was made in-house, based on the original method published in O. K. Andersen, Phys. Rev. B **12**, 3060 (1975) and has been used in, e.g., N. M. Rosengaard and B. Johansson, Phys. Rev. B **55**, 14975 (1997) and T. Eriksson, R. Lizárraga, S. Felton, L. Bergqvist, Y. Andersson, P. Nordblad, and O. Eriksson, *ibid.* **69**, 054422 (2004).
[27] U. von Barth and L. Hedin, J. Phys. C **5**, 1629 (1972).
[28] A. G. Kuchin, A. S. Ermolenko, V. I. Khrabrov, and G. M. Makarova, Phys. Status Solidi B **197**, 447 (1996).
[29] A. R. Mackintosh, Phys. Rev. Lett. **9**, 90 (1962).
[30] S. C. Keeton and T. L. Loucks, Phys. Rev. **168**, 672 (1968).
[31] P. Andersson, L. Nordström, and O. Eriksson, Phys. Rev. B **60**, 6765 (1999).
[32] R. Lizárraga, L. Nordström, L. Bergqvist, A. Bergman, E. Sjöstedt, P. Mohn, and O. Eriksson, Phys. Rev. Lett. **93**, 107205 (2004).